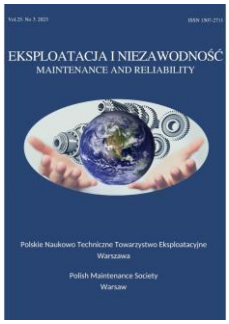

Eksploatacja i Niezawodnosc – Maintenance and Reliability
Volume 25 (2023), Issue 3
journal homepage: http://www.ein.org.pl

Article citation info:
Chen K, Yang C, Zhao Y, Niu P, Niu N. N, Wu H, Optimization of Square-shaped Bolted Joints Based on Improved Particle Swarm Optimization Algorithm, Eksploatacja i Niezawodnosc – Maintenance and Reliability 2023: 25(3)
http://doi.org/10.17531/ein/168487

Optimization of Square-shaped Bolted Joints Based on Improved Particle Swarm Optimization Algorithm

Indexed by: Web of Science Group

Kui Chen[a], Cheng Yang[b], Yongsheng Zhao[a,*], Peng Niu[a], NaNa Niu[a], Hongchao Wu[c]

[a] Faculty of Materials and Manufacturing, Beijing University of Technology, China
[b] Beijing Institute of Aerospace Control Devices, China
[c] XCMG Construction Machinery, China

Highlights

- Establish the dynamics model of square bolt connection based on fractal theory.
- An improved particle swarm optimization algorithm considering the influence of time-varying weight and contraction factor is proposed.
- Compared with the traditional algorithm, the improved optimization algorithm shows better operational performance.
- Meanwhile, the global stiffness optimization of the square bolt connection is realized.

Abstract

The bolted joint is widely used in heavy-duty CNC machine tools, which has huge influence on working precision and overall stiffness of CNC machine. The process parameters of group bolt assembly directly affect the stiffness of the connected parts. The dynamic model of bolted joints is established based on the fractal theory, and the overall stiffness of joint surface is calculated. In order to improve the total stiffness of bolted assembly, an improved particle swarm optimization algorithm with combination of time-varying weights and contraction factor is proposed. The input parameters are preloading of bolts, fractal dimension, roughness, and object thickness. The main goal is to maximize the global rigidity. The optimization results show that improved algorithm has better convergence, faster calculation speed, preferable results, and higher optimization performance than standard particle swarm optimization algorithm. Moreover, the global rigidity optimization is achieved.

Keywords
particle swarm optimization algorithm, bolt connection, bolted joint, fractal theory

1. Introduction

The heavy-duty CNC machine tools have a large number of joints, which not only break the continuity of machine structure, but also reduce the stiffness of the overall structure. According to statistics, the static stiffness of CNC machine is 30-50% depending on the joint stiffness, and 60% of the overall machine vibration is caused by joint parts. In the mechanical structure, joints exist in machined surfaces. Namely, there are many factors that influence the characteristics of joint surfaces, such as external load, material properties, processing methods, roughness, and structure type and size [1,2]. Therefore, the optimization of joint parameters is particularly critical for machine static and dynamic characteristics.

At present, the curve fitting method is used to determine joint parameters' numerical value. Many empirical formulas were proposed [3-6], but they are only suitable for small number of influencing factors, while they are intractable for multi-

(*) Corresponding author.
E-mail addresses: K. Chen:30699377@qq.com, C. Yang : yangchengappy@126.com, Y. Zhao:yszhao@bjut.edu.cn, P. Niu :niupeng100100@emails.bjut.edu.cn, N. N, Niu : 1542443055@qq.com, H. Wu : 15210181355@163.com,

influencing factors, wherein complex changes are needed. H Yu et al. [7] addressed the dynamic balance of milling cutters, which cannot be neglected in high-speed milling. Based on the particle swarm optimization (PSO) algorithm to optimize the spiral edge shape of the end mill, the radius of curvature of the spiral edge curve is optimized. The unbalance of the milling cutter is effectively reduced and the dynamic performance of the milling cutter is further improved. D Wen et al. [8] proposed a fast backfire double-annealing particle swarm optimization (FBDAPSO) based method for motor parameter identification. The accuracy and evolution speed are improved and the problem of redundant iterations of SAPSO is solved. SK Lu et al. [9] proposed a new method to calculate the stiffness of bolted joints. The influence of the joint surface stiffness on the overall stiffness was considered. An expression model of the stiffness characteristics of the joint surface was established. The stiffness of the bolted joint surface was effectively improved. W Liu et al. [10] constructed an AL-based ELM model based on fractal theory suitable for granular image features, and optimized the ELM model to obtain the optimal number of hidden layer neuron nodes for each mineral by predicting the feature parameters of granular images with the improved ELM algorithm. Based on RFPA2D and digital image processing techniques, L Zheng et al. [11] proposed a method to calculate the mesoscale fractal dimension of irregular rock particles. The effects of loading conditions and mesoscale heterogeneity on the damage of irregular sandstone particles were investigated. It is of great significance to explore the rock particle breaking and energy consumption laws, rock breaking mechanism, and to find an efficient and energy-saving rock breaking method. Liu et al. [12] proposed a nonlinear model of bolt pretightening force for optimizing the contact performance. Based on finite element simulation, Grzejda [13] studies the bearing capacity of a bolted connection fastener when a bolt is damaged. The quadratic regression mathematical model was employed by Xu et al. [14] to study the main working factors affecting attenuation of bolt preload under vibration. Wang et al. [15] used the spring damping element to simulate the contact characteristics of joint surface, and they established the finite element model of large thread grinder and optimized its static and dynamic characteristics. Cheng et al. [16] established the energy dissipation model of bolted joints based on the 2-dOF vibration differential mathematical model. Chen et al. [17] used the gradient method of unconstrained optimization to identify the stiffness and damping parameters of grinder fixed surface. Wei et al. [18] studied the estimation of furnace joint failure process by considering the influence of service life, service strength, maintenance and inspection. Wang et al. [19] proposed a compilation method for Comprehensive Smoothness Evaluation (G-SCE) based on kernel density estimation (KDE). KDE was applied to establish the dynamic cutting force distribution of CNC lathes without grouping the calculated load cycles. Wang et al. [20] obtained the dynamic parameters of key joint surface of milling machine based on the ANSYS software. Li et al. [21] used the simulated annealing algorithm to identify the kinetic parameters of bolted joint.

The neural network optimization mainly focuses on improvement of group intelligent optimization algorithm. Namely, the group intelligent optimization algorithm has become very important in artificial intelligence, and a large number of studies on this subject was published in academic magazines and journals. Based on artificial neural networks, Ramirez IS [22] proposed a new method for signal processing, fault detection, and diagnosis that combines statistical analysis and advanced algorithms. In addition, Abid M [23] studied the oil pipeline flange connection surface and bolt connection of fastening optimization strategy. Ibai Coria [24] proposed a new optimization method for fastening of bolt sequence for ring joints. Arumuga [25] proposed a new improved particle swarm optimization algorithm for optimization of global and local parameters, which improved both efficiency and accuracy. However, an optimization in the field of engineering design is more extensive, and a lot of joint parts of CNC machine need to be optimized in order to improve their overall stiffness and dynamic and static characteristics. At present, the most commonly used method is geometric optimization, wherein analysis follows modeling, and re-analyzing is involved according to requirements. However, this optimization process is mainly dependent on human experience, so there are many limitations. Moreover, the optimization process is complicated, which disables rapid obtaining of results.

In this paper, the fractal model of contact parameters of bolted joints is established by optimization of the high-strength bolts. The mathematical programming, parametric modeling

and a combinatorial improved particle swarm optimization algorithm are used to analyze and optimize the bolted joint parts based on intelligent optimization platform. By changing the component thickness, the overall characteristics of bolted joints are improved, and a high stiffness of joints is achieved.

2. Characteristic analysis of bolted joints

The bolt connection is very critical for the heavy duty machine tools, which plays a prominent role in fixation and support. Since, the joints have a considerable influence on the overall performance of CNC machines [26], it is very important to analyze joint surfaces. The relaxation characteristics of a high-strength bolted structure are affected both macroscopically and microcosmically by multi-factor coupling effects, which make the relaxation mechanism of high-strength bolted structure very complicated. Due to the rapid development of heavy duty CNC machine tools in terms of high precision, high reliability, multifunction and intelligence, the research on relaxation mechanism of high-strength bolted structures and its influence on precision of heavy duty machine tools are very imperative because these mechanisms have become basic and urgent problem for advanced heavy duty CNC machine tools manufacturing in terms of higher grade. This paper focuses on analysis of high-strength bolted structure in heavy-duty machine tools, Fig. 1.

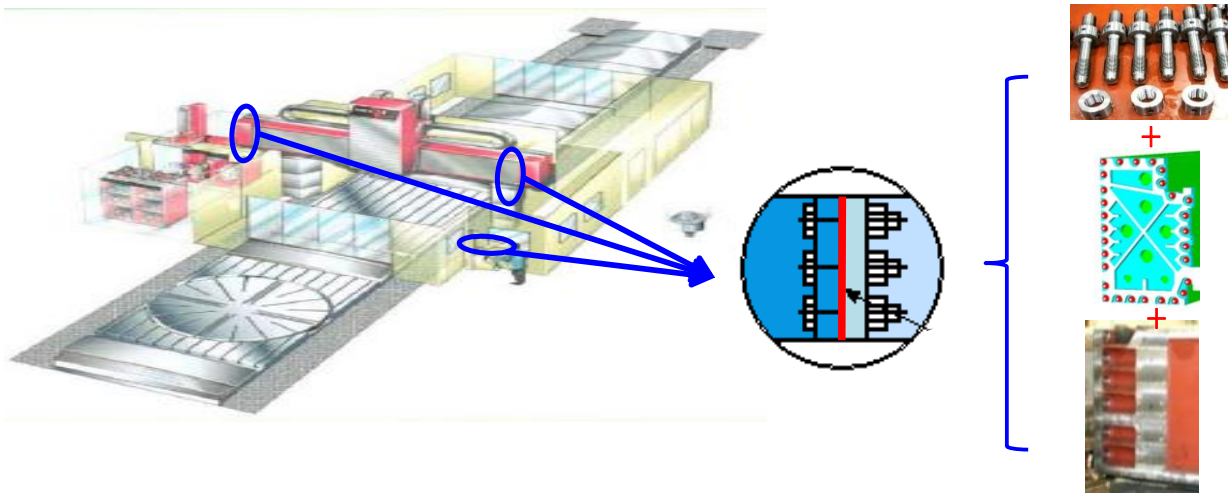

Fig. 1. High-strength bolted structure.

2.1 The influencing factors of joint

As it is well known, there are many factors that influence machine joints. A certain number of scholars have conducted numerous studies on dynamic characteristics of bolted joints. Among these dynamic characteristics, the typical unit parameters play a very important role in the machine structure dynamics [27]. The influencing factors of joints are mostly non-linear, and due to the diversification of use conditions the analysis becomes more complicated. The main influencing factors are:

(1) joint material and its properties (G, E, μ,ρ),
(2) joint processing method,
(3) surface roughness between bonding surfaces,
(4) joint static load (i.e. working surface pressure),
(5) joint structure, type, shape and size,
(6) joint dynamic force, and
(7) vibration frequency.

The above-mentioned factors can be summarized into three categories: the structure-related factors, such as joint type, shape and size; the inherent-characteristics factors, such as materials, construction methods and surface roughness; and, the relevant factors, such as combination state and vibration frequency.

In summary, the contact parameters of joint surfaces have a great influence on joint dynamic characteristics. Moreover, joint thickness, preload, number of bolts, distribution of bolts and contact surface morphology also have an effect on joint dynamic characteristics. However, this paper mainly analyzes the contact parameters of joint surface.

2.2 Modeling of joint surface

The characteristics of fixed joint surface relate to elastic and damping characteristics, energy storage and energy

consumption. In establishment of dynamic model of bolted joints, the quality of contact element is ignored and only its stiffness and damping are considered. Many scholars have proposed a lot of models that analyze contact stiffness of joint surface from a microscopic point of view [28-29], which mainly considers the normal contact stiffness. In this paper, the M-B fractal theory is used to study the nonlinear model of rough contact surface from the microscopic point of view. Namely, we analyze fractal characterization of rough surface, asperity contact model, and cross-sectional distribution function of contact asperity. The profile curve of rough surface can be expressed by Weierstrass-Mandelbrot function:

$$z(x) = G^{(D-1)} \sum_{n_1}^{n_{max}} \Sigma_n \left(\frac{\cos 2\pi\gamma^n x}{\gamma^{(2-D)n}}\right);\ 1<D<2\ ;\ \gamma>1 \quad (1)$$

where z is the contour height of rough surface, x denotes the coordinates of surface sampling length, D is the fractal dimension of contour curve, G is the feature scale coefficient of rough surface, γ is the size parameter of spectral density, and ϕ_n is a random phase.

The M-B fractal contact model considers the rough surface as isotropic and statistic. The contact of two rough surfaces is simplified by a model of an elastic rough surface with an ideal rigid smooth surface. The simplified contact model is shown in Fig. 2. The asperity contact model is shown in Fig. 3.

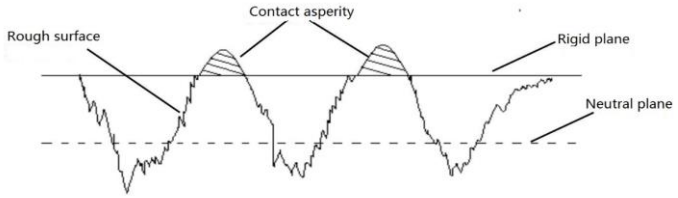

Fig.2. Simplified Contact Model of Rough Surface.

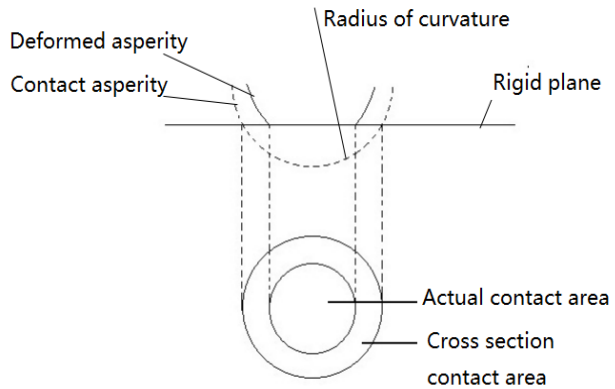

Fig. 3. Asperity Contact Model.

The morphology of a single asperity can be obtained from a single frequency ($\gamma^n = \frac{1}{l}$) W-M function, Fig. 4.

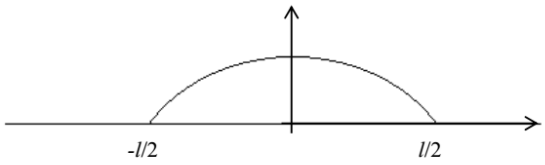

Fig. 4. Single asperity topography.

The corresponding mathematical formula is:

$$Z_0(x) = G^{D-1} l^{2-D} \cos\frac{\pi x}{l} \quad (2)$$

where D is the fractal modulus, which stands for the frequency of high and low composition of contour and it is in the range 1-2, $G$is the fractal roughness, which represents the contour height, the greater G is, the rougher surface is, $l$is the contact length of a single asperity in the range of x and it is from $-\frac{l}{2}$to $\frac{l}{2}$.

If we label the cross-sectional area of asperity as a', then deformation δ is obtained from $Z_0(x)$ when x is equal to 0:

$$\delta = Z_0(0) = G^{D-1} a'^{\frac{2-D}{2}} \quad (3)$$

At the microscopic scale, it can be considered that $a'$is equal to l^2. The apex radius of asperity is defined by:

$$R = \left\{\left|\frac{d^2 Z_0(x)}{dx^2}\right|\right\}^{-1} = \frac{a'^{\frac{D}{2}}}{\pi^2 G^{D-1}} \quad (4)$$

According to the Hertz theory, the critical conditions for deformation are defined by:

$$\delta_c = \left(\frac{\sigma_y K\pi}{2E}\right)^2 R = \left(\frac{H}{2E}\right)^2 \frac{a'^{\frac{D}{2}}}{G^{D-1}} \quad (5)$$

where δ_c is the yield strength of softer material, H is the hardness of softer material, K is the scale factor, and E is the equivalent elastic modulus of contact materials, and it is defined by:

$$\frac{1}{E} = \frac{1-v_1}{E_1} + \frac{1-v_2}{E_2} \quad (6)$$

where E_1, E_2 and v_1, v_2 represent the elastic modulus and Poisson's ratio of contact materials, respectively.

If δ is equal to δ_c, the critical contact area can be obtained by:

$$a'_c = G^2 \left(\frac{2E}{H}\right)^{\frac{2}{D-1}} \quad (7)$$

It can be seen in Eq.7 that a'_c is a fixed value in the case

when surfaces roughness is determined. According to the Hertz theory, the elastic load and plastic load of a single asperity are $F_e = \frac{4Er^3}{3R}$ and $F_p = Ha'$, respectively, where r is the radius of the real contact surface.

Furthermore:

$$a = \pi r^2 = \frac{a'}{2} \tag{8}$$

According to (8) and $F_e = \frac{4Er^3}{3R}$ we get:

$$F_e = \frac{4}{3}\sqrt{\pi}EG^{D-1}\left(\frac{a'}{2}\right)^{\frac{3-D}{2}} \tag{9}$$

In M-B model, the relationship between number of asperity contact points and cross-sectional area is defined by:

$$n(a') = \frac{Da_L'^{\frac{D}{2}}}{2a'^{\frac{D}{2}+1}} \tag{10}$$

where a_L' is the maximal contact area, and $n(a')$ is the density function of contact area distribution.

Then, the total elastic contact load and plastic contact load of joint surfaces can be expressed by (11) and (12), respectively:

$$P_e = \int_{a_C'}^{a_L'} F_e\, n(a')da' = \frac{4\sqrt{\pi}EDG^{D-1}}{3(3-2D)}a_L'^{\frac{D}{2}}\left(a_L'^{\frac{3-2D}{2}} - a_C'^{\frac{3-2D}{2}}\right) \tag{11}$$

$$P_p = \int_0^{a_C'} F_p\, n(a')da' = \frac{HD}{2-D}a_L'^{\frac{D}{2}}\left(a_L'^{1-D} - a_c'^{1-D}\right) \tag{12}$$

Consequently, the total surface normal load model is determined by:

$$P = \begin{cases} P_e + P_p & a_L' > a_c' \\ P_p & 0 < a' < a_c' \end{cases} \tag{13}$$

Assuming that pressure between joint surfaces has a uniform distribution, the equivalent pressure of joint surface can be expressed by:

$$\bar{P} = \frac{P}{A_a} \tag{14}$$

The dynamic parameters of bolted joint include stiffness and damping, wherein stiffness and damping are calculated in xy, y and z directions. According to the definition of stiffness, the normal contact stiffness of a single asperity can be obtained by:

$$k_n = \frac{dF_e}{d\delta} = \frac{2^{\frac{D+1}{2}}(3-D)E^*}{3\sqrt{\pi}(2-D)}a'^{\frac{1}{2}} \tag{15}$$

If (15) is combined with the cross-sectional area distribution function, the total stiffness of joint is defined by:

$$K_n = \int_{a_c'}^{a_L'} k_n n(a')\, da' = \frac{2^{\frac{D+1}{2}}(3-D)E^*D\psi^{\frac{2-D}{2}}}{3\sqrt{\pi}(2-D)(1-D)}a_L'^{\frac{1}{2}}\left(a_L'^{\frac{1-D}{2}} - a_c'^{\frac{1-D}{2}}\right) \tag{16}$$

The ANSYS software was used to simulate static parameters for different preloading conditions, and contact pressure of each node was extracted. Then, according to the contact pressure of joint surfaces, normal contact stiffness and contact damping of each node were obtained by MATLAB algorithm. Finally, contact stiffness and damping level of the corresponding nodes were established using matrix elements of finite element algorithm. The natural frequency and vibration modes were extracted using free modal analysis, and the harmonic response was obtained by harmonic response analysis.

According to simulation results it can be concluded that pressure distribution of joint surface is not uniform for different bolt preloads. Namely, in the vicinity of bolt, the stress is the most uneven and far higher than in other areas, and in the areas that are away from the bolt, the stress is relatively small and distribution is relatively uniform. The dynamic characteristics of bolted joint reflect the influence of contact parameter on bolted joint. On the other hand, vibration characteristics of bolted joint include natural frequency and main vibration mode, which can be obtained by finite element modal analysis. The greater the contact stiffness is, the better the effectiveness of contact is, and the higher natural frequency is.

3. Improved particle swarm optimization algorithm

The Particle Swarm Optimization (PSO) algorithm mimics the foraging behavior of birds, wherein the search space problem is equated to the flying space of birds, and each bird is abstracted as a mass-free, volume-free particle. The PSO is used to express a candidate solution. The optimal solution is equivalent to the objects that birds are looking for. The basic idea is to determine the global optimal solution by cooperation and information sharing among individuals in population. Compared with other evolutionary algorithms, PSO algorithm has the advantages of simplicity, easy implementation, stronger global optimization, fast convergence, high robustness, and strong global searching ability. Moreover, there is no choice, intersection, mutation, and other evolutionary operations compared to the genetic algorithm, which can shorten training period of neural network.

3.1 Basic particle swarm optimization algorithm

In D-dimensional space, where a population $x =$

$(x_1, x_2 \cdots, x_m)^T$ is formed from the quantity of m particles, the position and velocity of the i^{th} particle are $x_i = (x_{i,1}, x_{i,2}, \cdots, x_{i,D})^T$ and $v_i = (v_{i,1}, v_{i,2}, \cdots, v_{i,D})^T$, respectively. During each iteration, the particles are updated by searching for optimal solution; the first is the optimal solution found by particle itself - the individual extreme p_{best} $p_i = (p_{i,1}, p_{i,2}, \cdots, p_{i,D})^T$, and the other is the optimal solution found within the whole population - the global optimal solution g_{best} $p_g = (p_{g,1}, p_{g,2}, \cdots, p_{g,D})^T$. During the searching for these two optimal solutions, the particle is iterated by:

$$v_{i,d}^{k+1} = v_{i,d}^k + c_1 r_1 (p_{i,d}^k - x_{i,d}^k) + c_2 r_2 (p_{g,d}^k - x_{i,d}^k) \quad (17)$$

$$x_{i,d}^{k+1} = x_{i,d}^k + v_{i,d}^{k+1} \quad (18)$$

Where c_1 and c_2 are the positive learning factors, r_1 and r_2 are evenly distributed random numbers in the range 0-1, $v_{i,d}^k$ is the velocity of particle d in the k^{th} iteration, $x_{i,d}^k$ is the position of particle $d$in the k^{th} iteration, $p_{i,d}^k$ is the position of individual i in D-dimensional space of particle, and $p_{g,d}^k$ is the position of global extreme value of particle i in D-dimensional space.

3.2 Improved particle swarm optimization algorithm

3.2.1 Improved particle swarm optimization algorithm with time-varying weight

The basic PSO algorithm has a problem with convergence to the optimal solution. The improved algorithm can accelerate the convergence and improve the quality of solution. The commonly used improved algorithm is based on the inertia weight algorithm defined by:

$$v_{i,d}^{k+1} = \omega v_{i,d}^k + c_1 r_1 (p_{i,d}^k - x_{i,d}^k) + c_2 r_2 (p_{g,d}^k - x_{i,d}^k) \quad (19)$$

$$x_{i,d}^{k+1} = x_{i,d}^k + v_{i,d}^{k+1} \quad (20)$$

Where, ω is the inertia weight. However, the fixed weight is commonly used, so ω is the constant between 0 and 1. However, when problem becomes more complex, the performance of fixed weight algorithm related to the searching for optimal solution decreases. Thus, the improved optimization algorithm with time-varying weight is introduced:

$$v_{i,d}^{k+1} = \omega_i v_{i,d}^k + c_1 r_1 (p_{i,d}^k - x_{i,d}^k) + c_2 r_2 (p_{g,d}^k - x_{i,d}^k) \quad (21)$$

$$x_{i,d}^{k+1} = x_{i,d}^k + v_{i,d}^{k+1} \quad (22)$$

where the inertia weight varies between ω_{min} and ω_{max}. If the maximal number of iterations is labeled as M_{Iter}, then, the inertia weight of the i^{th} iteration is defined by:

$$\omega_i = \omega_{max} - \frac{\omega_{max} - \omega_{min}}{M_{Iter}} \times i \quad (23)$$

ω decreases linearly, and when ω gradually decreases the particle speed also decreases, which accelerates the particle convergence speed and improves the optimization performance.

3.2.2 Improved particle swarm optimization algorithm with shrinkage factor

Clerc introduced the concept of shrinkable factor in the basic particle swarm algorithm, which can ensure the convergence of particle swarm algorithm by controlling the inertia weight and value of learning factor. The improved algorithm is defined by:

$$v_{i,d}^{k+1} = K\left[v_{i,d}^k + c_1 r_1 (p_{i,d}^k - x_{i,d}^k) + c_2 r_2 (p_{g,d}^k - x_{i,d}^k)\right] \quad (24)$$

$$x_{i,d}^{k+1} = x_{i,d}^k + v_{i,d}^{k+1} \quad (25)$$

where the contraction factor K is the function of c_1 and c_2, and it can be expressed by:

$$K = \frac{2}{\left|2 - \varphi - \sqrt{\varphi^2 - 4\varphi}\right|}, \varphi = c_1 + c_2 > 4 \quad (26)$$

In the Clerc's shrinkage factor method, φ is usually equal to 4.1, thus, K is equal to 0.729.

3.2.3 Improved particle swarm optimization with combination of time-varying weight and shrinkage factor

Considering the advantages of above-mentioned PSO algorithm improvements, a new combinatorial improved optimization algorithm, which can both accelerate convergence and improve solution quality, is proposed. In order to guarantee the convergence of particle swarm algorithm, we introduce the algorithm presented in Fig. 5, which is defined by:

$$v_{i,d}^{k+1} = K\left[\omega_i v_{i,d}^k + c_1 r_1 (p_{i,d}^k - x_{i,d}^k) + c_2 r_2 (p_{g,d}^k - x_{i,d}^k)\right] \quad (27)$$

$$x_{i,d}^{k+1} = x_{i,d}^k + v_{i,d}^{k+1} \quad (28)$$

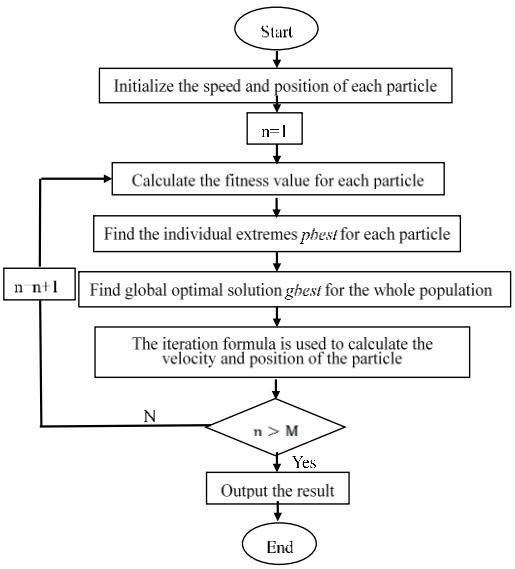

Fig. 5. Flowchart of proposed algorithm.

3.3 Optimization strategy

When the optimization algorithm is used to search for the optimal solution of fixed joints, the stiffness parameters affect natural frequency, modal shape and vibration amplitude of joint surface. In order to achieve the highest stiffness, the stiffness parameters of both joint surface and bolt are considered. In the optimization strategy, the input variables are thickness of square-shaped component, number of bolts, bolt preload force, fractal dimension and roughness. The objective function is stiffness of the whole. The whole optimization process is based on the following steps (Fig. 6):

(1) Set the necessary settings for APDL file generated by ANSYS and code file generated by MATLAB.

(2) Use the integrated optimization algorithm and set objective function, boundary conditions and parameter range.

(3) Start the optimization algorithm and run it until the termination condition is met.

(4) Output the result.

The above processes should be repeated several times to get the desirable optimization results.

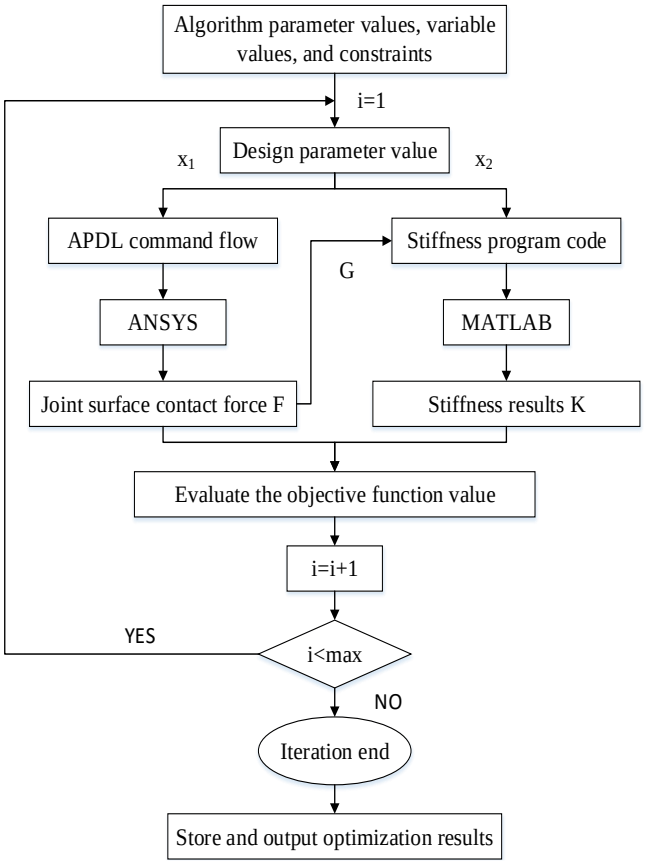

Fig. 6. Optimization flow chart.

4. Application examples

In this chapter, the square-shaped components connected by bolts in heavy duty CNC machine tools are studied.

First, ANSYS simulation software was used for static analysis in order to get the corresponding nodal pressure, and then contact stiffness of each node was calculated by MATLAB. Using the combinatorial improved optimization algorithm, the parameters such as thickness, preload and number of bolt holes were optimized to achieve the maximal stiffness of joints.

4.1 Structure modeling and analysis

The square-shaped structure material was QT600-3, and machining precision of two contact surfaces was 1.6 μm. The material properties are shown in Table 1.

Table 1. Material properties

Parameter	Value
Material density	7800 Kg/m3
Elasticity modulus	1.5E11 Pa
Poisson's ratio	0.3
Rigidity	1.96E9 Pa

We used two frame-like components connected by a plurality of bolts, which are shown in Fig. 7, wherein the main dimensions are provided.

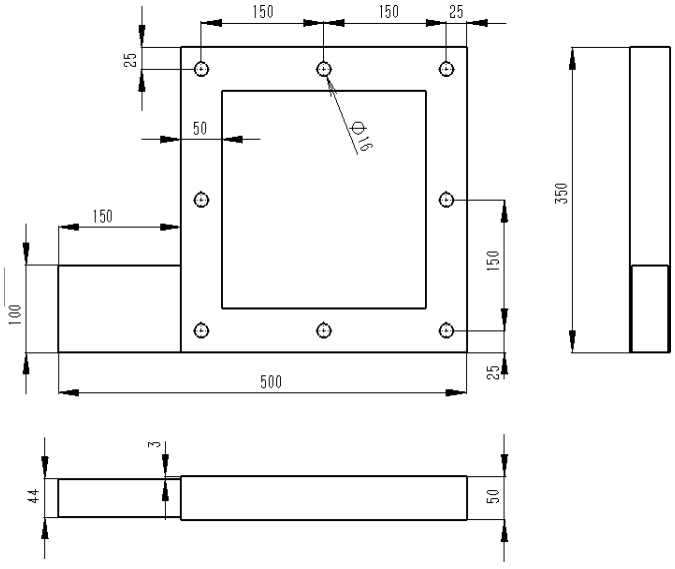

Fig. 7. Structure dimensions.

To better illustrate the bolt preload, we define the sequence of bolt tightening. The sequence of bolt tightening is shown in Fig. 8.

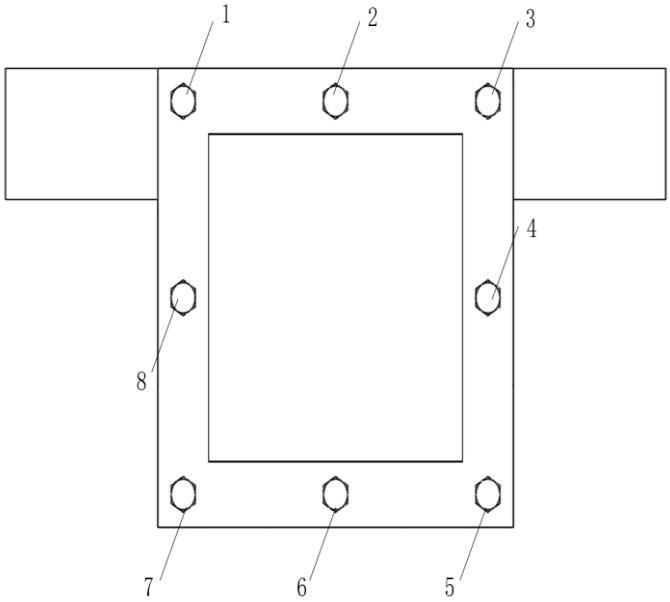

Fig. 8. Sequence of bolt tightening.

In order to achieve a high rigidity of bolt joint, the square-shaped structure was analyzed by changing of its thickness H, preload force F, fractal dimension D and roughness G. The static analysis was performed by ANSYS. The finite element model was used to load and obtain node information, then the node information was extracted to calculate contact stiffness of each joint. The modeling process mainly included geometric modeling, defining of types and attributes, defining of material properties, and meshing. The contact pressure was the largest at the structure edge. The pressure near the bolt was much larger than in other areas, and the pressure of bolts at four corners of structure was greater than ones in the middle of structure. Both ANSYS classic interface and APDL (ANSYS parametric design language) were used to obtain static analysis and dynamic analysis in order to facilitate data transfer between static and dynamic analyses. Finally, the APDL program file was generated. Using the APDL file, pressure of each node was obtained. Moreover, according to the fractal theory, stiffness of each node was calculated.

4.2 Finite Element Simulation

ANSYS was used to perform the finite element simulation. A hexahedron is used for meshing. The meshing results of the components are shown in Fig. 9. There are 332,935 nodes and 86,146 elements. The preload force of the bolts is 9000N and 10000N, respectively. Equal preload force is applied to each bolt. The simulation of the static structure under prestressing condition is performed first. Then, the modal simulation of the bolted members is carried out according to the results of the static structural simulation, and the first six orders of modal data of the members are obtained.

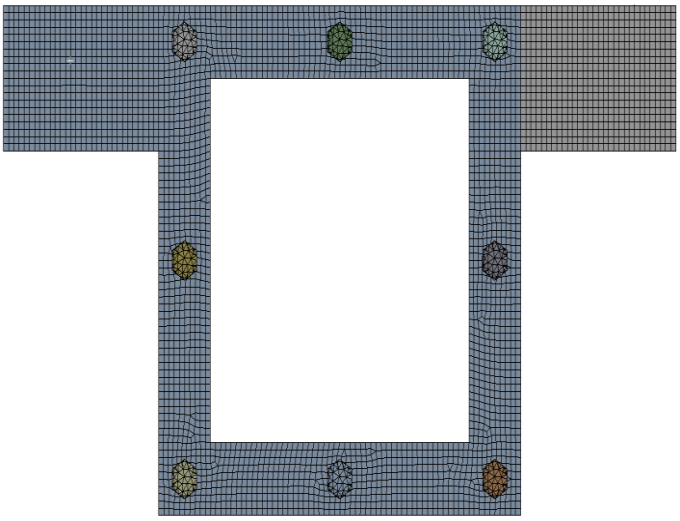

Fig. 9. Bolted connection construction meshing results.

When the preload force of the bolt is 9000N, the simulation results of the static structure of the member are shown in Fig. 10. From the simulation results, the maximum stress is 54.421 MPa. The stress distribution at each bolt connection is shown in Fig. 10.

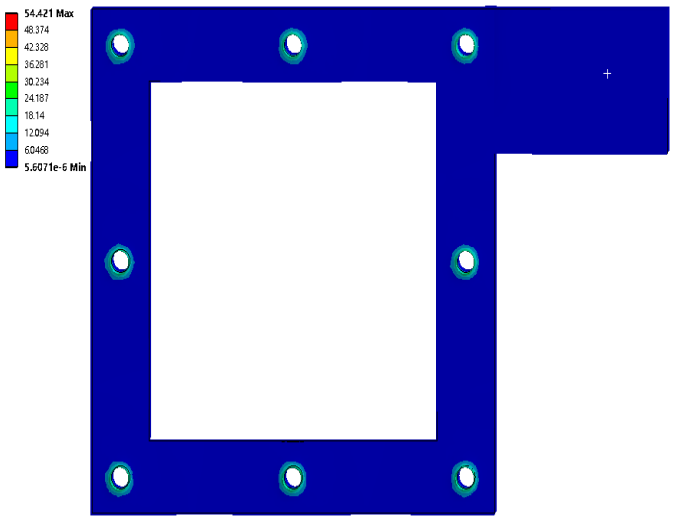

Fig. 10. Simulation results of the static structure when the preload force is 9000N.

Modal simulation based on static structure simulation. The deformation of each order of mode is shown in Fig. 11. The frequencies of each order of modes are shown in Table 2.

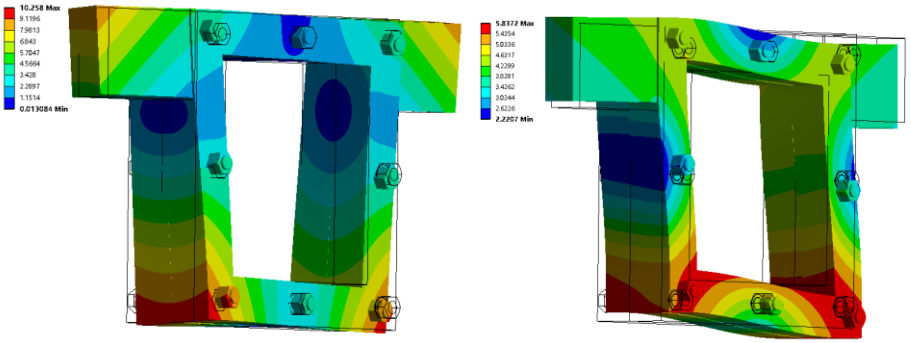

a) First order modal b) Second order modal

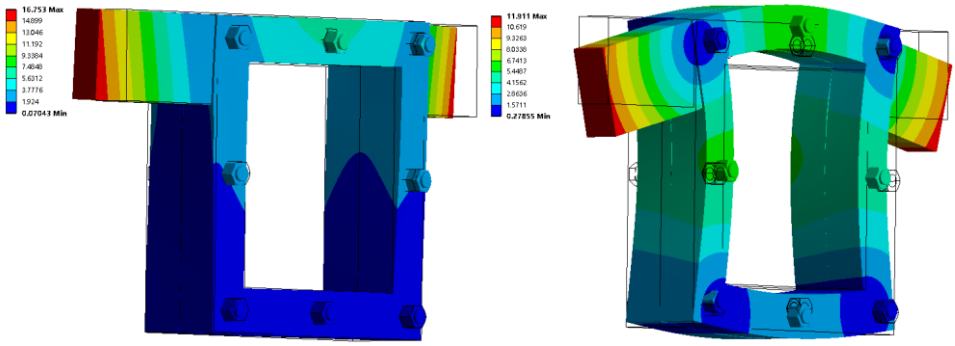

c) Third order modal d)Fourth order modal

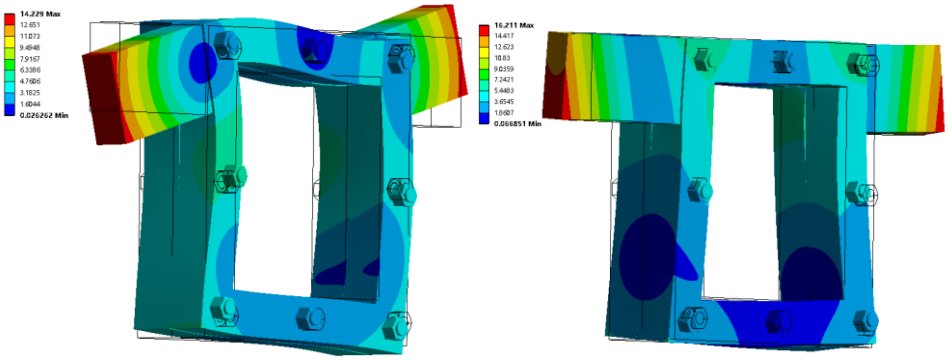

e) Fifth Order Modal f) Sixth order modal

Fig. 11. Modal simulation results when the preload force is 9000N.

Table 2. Frequency of each order of modal when the preload force is 9000N.

Number of steps	Frequency (Hz)
1	430.07
2	554.12
3	707.94
4	727.37
5	1115.6
6	1141.7

The simulation results of the static structure when the preload force is 10000N are shown in Fig. 12. According to the simulation results, the maximum stress is 79.934 MPa. The simulation results for each order of modalities are shown in Fig. 13. The frequencies of each order of modal is shown in Table 3.

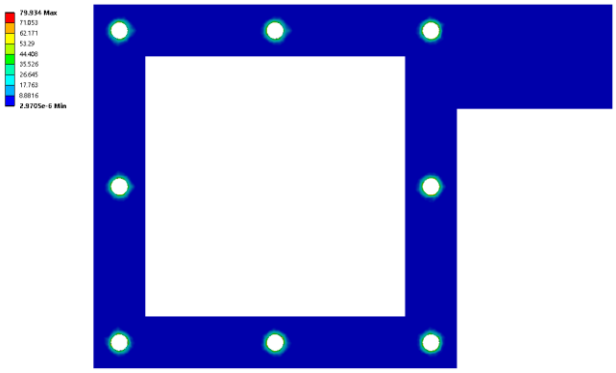

Fig. 12. Simulation results of the static structure when the preload force is 10000N.

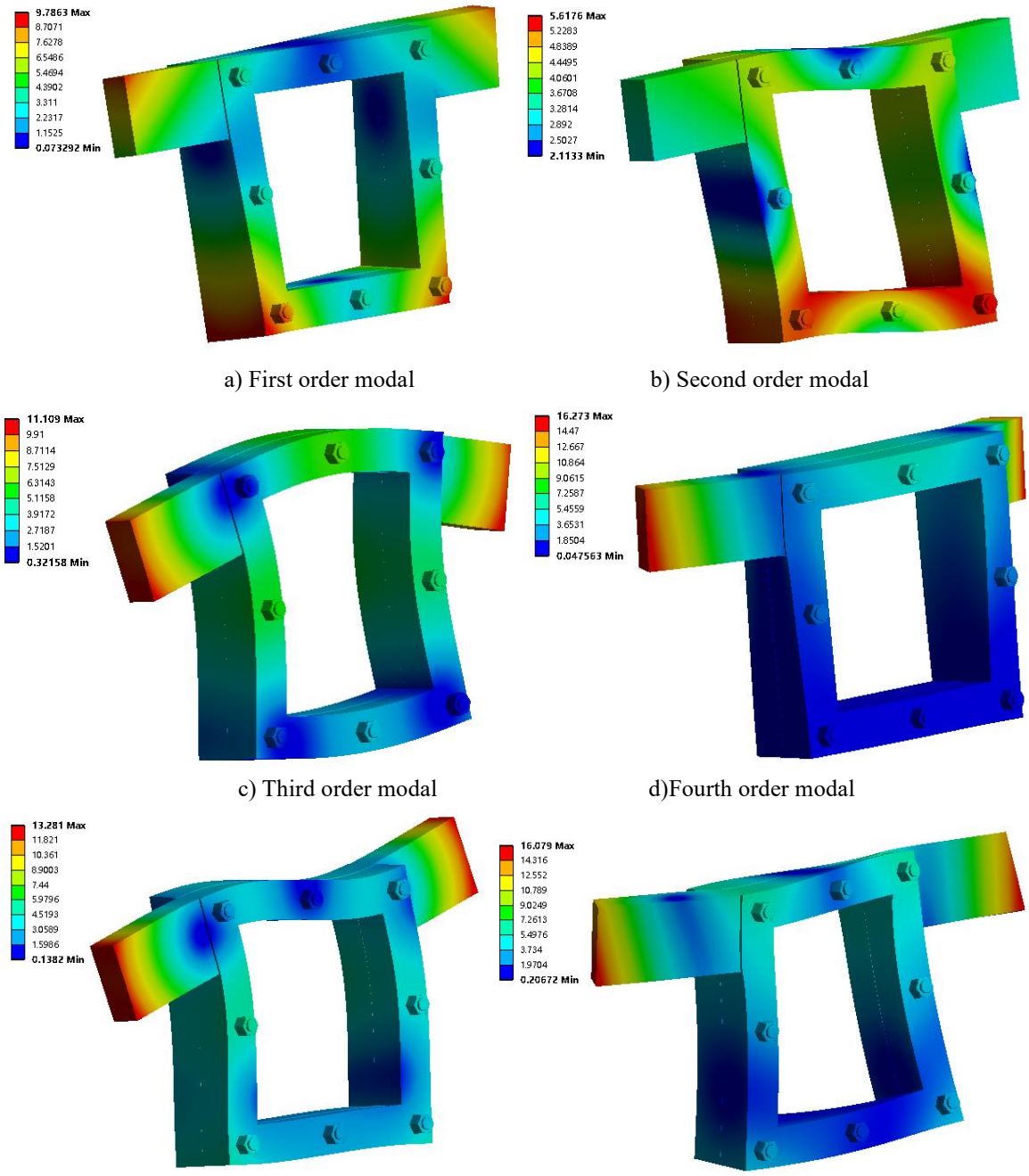

a) First order modal b) Second order modal

c) Third order modal d)Fourth order modal

e) Fifth Order Modal f) Sixth order modal

Fig. 13. Modal simulation results when the preload force is 10000N.

Table 3. Frequency of each order of modal when the preload force is 10000N.

Number of steps	Frequency (Hz)
1	648
2	724.16
3	951.31
4	986.72
5	1496.5
6	1622

4.3 Optimization results

The optimization results relate to the comparison of standard particle swarm (PSO) algorithm and improved particle swarm (MPSO) algorithm. The input parameters in both cases were preload force in 8 different positions $F_1 - F_8$, fractal dimension D, roughness G and thickness H, and the output was total stiffness K_{all} of square-shaped structure joint. The boundary conditions for input parameters are shown in Table 2.

Table 4. The boundary conditions for input parameter.

Parameter type	Lower boundary	Input value	Upper boundary
Force1(N)	1000	9000	10000
Force2(N)	0	9000	10000
Force3(N)	1000	9000	10000
Force4(N)	0	9000	10000
Force5(N)	1000	9000	10000
Force6(N)	0	9000	10000
Force7(N)	1000	9000	10000
Force8(N)	0	9000	10000
D	1.2	1.2	1.6
G	1.0E-10	1.0E-10	1.0E-9
Thickness(mm)	30	50	60

For both standard particle swarm algorithm and improved particle swarm algorithm, all basic parameters were the same, namely, maximal number of iterations was set to 50, number of particles was 20, sum of iterations of particle swarm was equal to 1000, learning factors c_1 and c_2 were equal to 2, both global and local increments were 0.9 and maximal speed was 0.01. Two important solution parameters were added to the improved particle swarm algorithm, namely the initial value of inertia weight and the contraction factor K, which were 0.002 and 0.729, respectively. The iterative processes of standard and improved particle swarm algorithms are presented in Fig. 14 and Fig. 15, respectively.

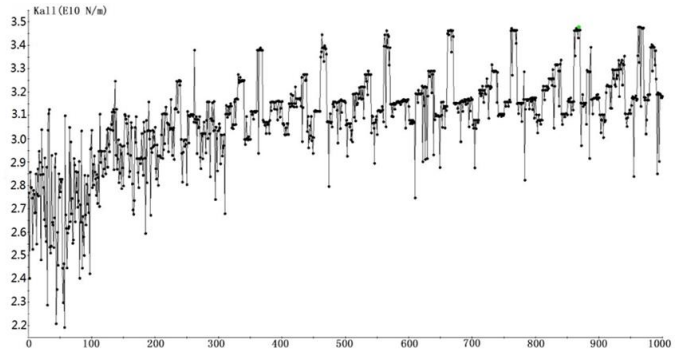

Fig. 14. Standard particle swarm algorithm.

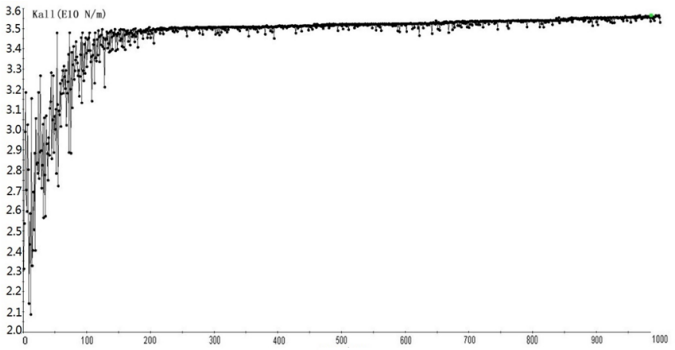

Fig. 15. Improved Particle Swarm algorithm.

According to the above two graphs, it can be concluded that improved PSO algorithm has better convergence than standard PSO algorithm. The improved algorithm found the optimal value K_{all} near the 300^{th} iteration, and the performance of searching for optimal solution is far higher than in the case of standard PSO algorithm. As it is shown in Table 5, the overall stiffness is the greatest when the preload and thickness are shown in Tab. 5, respectively.

Table 5. The optimal results.

Parameter type	The optimal value	Parameter type	The optimal value
Force1 (N)	7222	Force7(N)	8587
Force2(N)	8785	Force8(N)	8897
Force3(N)	5668	D	1.59
Force4(N)	4836	G	2.29E-10
Force5(N)	7093	Thickness(m)	0.05
Force6 $N)$	7636	K_{all} $(\frac{N}{m})$	3.5380E10

In order to present the particle swarm optimization process more intuitively, in Fig.16, preload is presented on x -axis, thickness is presented on y -axis, and total stiffness is presented on z -axis. The optimization process of the entire particle group can be seen from the latitude and color in three-dimensional map (Fig. 16). The darker the color is, the closer the solution is to the optimal solution. At the beginning, only a few particles are far away from the optimal solution, and most of them iterate near the optimal value.

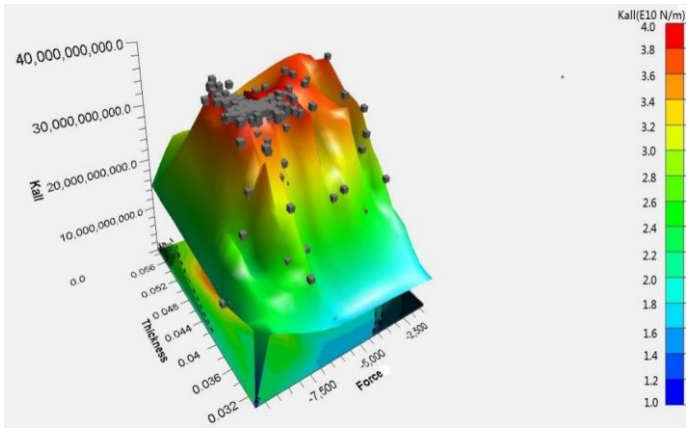

Fig. 16. Improved particle swarm optimization algorithm.

In order to verify stability and accuracy of improved algorithm, the improved particle swarm optimization algorithm was used for another 1000 iterations, and final optimization of total particle swarm was obtained after 2000 iterations. The results are shown in Table 6.

Table 6. Optimization results.

Parameter type	The optimal value	Parameter type	The optimal value
Force1(N)	6654	Force7(N)	6068
Force2(N)	7558	Force8(N)	5180
Force3(N)	9033	D	1.59
Force4(N)	5886	G	1.00E-10
Force5(N)	3982	Thickness(m)	0.04
Force6(N)	6321	K_{all} $(\frac{N}{m})$	3.5380E10

5. Conclusion

A new improved particle swarm optimization algorithm based on the fractal theory of joint surfaces, which aims to the optimization of joints' parameters, is proposed. By changing component thickness, bolt preload, surface topography and other parameters, the overall joint contact stiffness is optimized. According to the results, it can be concluded that improved algorithm has better convergence, faster searching speed, and better performance than basic particle swarm optimization algorithm. In simulations, the improved algorithm found optimal solution after 1,000 iterations, and then another 1,000 iterations were conducted in order to verify algorithm stability. The optimal value of both algorithms was basically the same, which indicates that improved algorithm is stable and accurate, and that optimization of total stiffness of joints is successfully achieved.

Funding

The author(s) disclosed receipt of the following financial support for the research, authorship, and/or publication of this article: This work was supported by the National Natural Science Foundation of China (No.52075012) and the Open Fund of Aerospace Servo Drive and Transmission Technology Laboratory (LASAT-20210103).

References

1. Abid M, Khan A, Nash DH, Wajid HA. Simulation of Optimized Bolt Tightening Strategies for Gasketed Flanged Pipe Joints. Pressure Vessel Technology: Preparing For The Future. Vol. 130. 2015; 204-213, https://doi.org/ 10.1016/j.proeng.2015.12.210 .
2. Arumugam MS, Rao MVC and Chandramohan A. A new and improved version of particle swarm optimization algorithm with global-local best parameters. Knowledge And Information Systems, 2008;16(3): 331-357, https://doi.org/10.1007/s10115-007-0109-z.
3. Cheng Q, Xu WX, Liu ZF, Yang CB,Li Y. The Effects of Energy Dissipation of the Closure Bolted Joints Under Vibration Behavior. Journal of Pressure Vessel Technology-Transactions of The Asme, 2021; 143(2); https://doi.org/10.1115/1.4048072.
4. Epstein M and Adeeb SM. The stiffness of self-similar fractals. International Journal Of Solids And Structures, 2008;45(11-12):3238-3254, https://doi.org/10.1016/j.ijsolstr.2008.01.022 .
5. Garland PP and Rogers RJ. An Experimental Study of Contact Forces During Oblique Elastic Impact. Journal Of Applied Mechanics-Transactions Of The Asme, 2009; 76(3), https://doi.org/10.1115/1.3063634.
6. Goerke D and Willner K. Normal contact of fractal surfaces - Experimental and numerical investigations. WEAR, 2008;264(7-8): 589-598, https://doi.org/10.1016/j.wear.2007.05.004.
7. Grzejda R. Thermal strength analysis of a steel bolted connection under bolt loss conditions. Eksploatacja i niezawodnosc-maintenance and reliability, 2022; 24(2): 269-274, https://doi.org/10.17531/ein.2022.2.8.
8. Hu W, Westerlund P, Hilber P, Chen CH, Yang ZJ. A general model, estimation, and procedure for modeling recurrent failure process of high-voltage circuit breakers considering multivariate impacts. Reliability engineering & system safety, 2022;220, https://doi.org/10.1016/j.ress.2021.108276.
9. I Coria, Abasolo M, Olaskoaga I, Etxezarreta A, Aguirrebeitia J. A new methodology for the optimization of bolt tightening sequences for ring type joints. Ocean engineering, 2017;129: 441-450, https://doi.org/ 10.1016/j.oceaneng.2016.10.049.
10. Jiang SY, Zheng YJ and Zhu H. A Contact Stiffness Model of Machined Plane Joint Based on Fractal Theory. Journal Of Tribology-Transactions Of The Asme, 2010; 132(1): https://doi.org/10.1115/1.4000305.
11. Li DS, Zhang YD , and Wang P. Dynamic model of machine joints based on structural damping. Journal of Vibration and Shock ,2010; 29(8):204-208.
12. Liu HB, Wu JK, Liu K, Kang K, Luo Q,Liu ZS, Wang YQ. Pretightening sequence planning of anchor bolts based on structure uniform deformation for large CNC machine tools. International Journal of Machine Tools & Manufacture: Design, research and application ,

2019；136：1-18, https://doi.org/ 10.1016/j.ijmachtools.2018.09.002.

13. Lu SK,Hua DX, Li Y, Cui FY, Li PY. Stiffness Calculation Method and Stiffness Characteristic Analysis of Bolted Connectors. Mathematical Problems in Engineering ,2019; https://doi.org/10.1155/2019/6206092.
14. Liu WX, Yan SH, Chen TL, Cheng JQ, Wang K, Song JT, Yang AM, Li J, Xing HW, Zhang YZ. Feature recognition of irregular pellet images by regularized Extreme Learning Machine in combination with fractal theory. Future Generation Computer Systems ， 2022；127:92-108, https://doi.org/10.1016/j.future.2021.08.003.
15. Liu YL, Bo SG and Xu ZL. A friction contact stiffness model of fractal geometry in forced response analysis of a shrouded blade. Nonlinear Dynamics, 2012;70(3): 2247-2257, https://doi.org/10.1007/s11071-012-0615-8.
16. Liu ZF, Wang YZ, Dong XM, Zhang CX, Li Y. et al. A novel model for evaluating preload based on spectral problem in system with double-bolted connections. Applied Mathematical Modelling, 2022;102: 21-34, https://doi.org/10.1016/j.apm.2021.09.016.
17. Nan J. Modeling and correcting fem with contact element for the combined surfaces of grinder bolts. China Mechanical Engineering 2001.
18. Niu NN, Zhao YS, Li Y , Chen K, Li X. Contact modeling of heterogeneous materials of the machine tool bed-foundation interface based on the gradient of contact stress distribution. Journal of the Brazilian Society of Mechanical Sciences and Engineering,2022; 44(12), 1-16, https://doi.org/10.1007/s40430-022-03910-3.
19. Niu P, Cheng Q, Zhang T, Yang CB, Zhang ZL, Liu ZF. Hyperstatic mechanics analysis of guideway assembly and motion errors prediction method under thread friction coefficient uncertainties. Tribology International, 2023;180, https://doi.org/10.1016/j.triboint.2023.108275.
20. Ramirez IS, Mohammadi-Ivatloo B, and Marquez F.Alarms management by supervisory control and data acquisition system for wind turbines. Eksploatacja i niezawodnosc-maintenance and reliability, 2021; 23(1): 110-116, https://doi.org/ 10.17531/ein.2021.1.12.
21. Shi JP, Ma K and Liu ZQ. Normal Contact Stiffness on Unit Area of a Mechanical Joint Surface Considering Perfectly Elastic Elliptical Asperities. Journal Of Tribology-Transactions Of The Asme, 2012; 134(3), https://doi.org/ 10.1115/1.4006924.
22. Wang LH, Luo JP, Liu HB, Huang YY. Research on dynamic characteristics of key machine joint surfaces of the numerically controled milling machine. Journal of Vibration and Shock 2008.
23. Wang SX, He JL, Li GF,Hao QB, Huang H. Compilation method of CNC lathe cutting force spectrum based on kernel density estimation of G-SCE. International journal of advanced manufacturing technology, 2023;124(11-12): 3713-3724, https://doi.org/ 10.1007/s00170-021-07541-1.
24. Wang YL, Wu XF, Feng HT. Static and dynamic characteristics optimization for a whole large-sized thread grinder based on joint surface. Journal of Vibration and Shock 2012.
25. Wen DD, Shi CD, Liao KX, Liu JH,Zhang Y. Fast Backfire Double Annealing Particle Swarm Optimization Algorithm For Parameter Identification Of Permanent Magnet Synchronous Motor. Progress In Electromagnetics Research ,2021;104:23-38, https://doi.org/10.2528/PIERM21052802.
26. Xu WX, Cheng Q, Yang CB, Li Y. Dynamic analysis and looseness evaluation of bolted connection under vibration of machine tools. International Journal of Advanced Manufacturing Technology, 2023; 124(11-12): 3761-3770, https://doi.org/10.1007/s00170-021-07615-0.
27. Yu HB, Zheng ML, Zhang W, Nie WY, Bian TC. Optimal design of helical flute of irregular tooth end milling cutter based on particle swarm optimization algorithm. Proceedings of the Institution of Mechanical Engineers, Part C. Journal of mechanical engineering science, 2022;236(7),3323-3339, https://doi.org/ 10.1177/09544062211042052.
28. Zheng LJ, Zheng LL, Zuo YJ, Liu H, Chen B, Wu ZH, Sun WJB, Wang YL. Study on Mesoscale Damage Evolution Characteristics of Irregular Sandstone Particles Based on Digital Images and Fractal Theory. Hindawi Limited, 2021, https://doi.org/ 10.1155/2021/6552847 .